Corrosion Science, Vol. 20, pp. 563 to 586
Pergamon Press Ltd. 1980. Printed in Great Britain.

THE CHARACTERISTICS OF THE POTENTIODYNAMIC POTENTIAL/CURRENT PROFILES OBTAINED WITH THE Ni/0.5 N H_2SO_4 INTERFACE. A CONTRIBUTION TO THE MECHANISM OF THE ELECTRODE PROCESS*

S. G. REAL, J. R. VILCHE and A. J. ARVÍA

Instituto de Investigaciones Fisicoquímicas Teóricas y Aplicadas, División Electroquímica, Sucursal 4—Casilla de Correo 16, 1900 La Plata, Argentina

Abstract—Electrochemical data derived from different simple and complex potentiodynamic techniques for the Ni/0.5 N H_2SO_4 interface furnish a new insight about the activation and initial stage passivation of nickel. The anodic dissolution of nickel involves a metal surface which is either partially or completely covered by species such as NiOH, [NiOH.$Ni(OH)_2$] or [$Ni(OH)_2$.NiOOH]. The chemical dissolution of the various species in the acid electrolyte occurs at different rates. The relative dissolution rates can be estimated from the data derived from the complex triangular potential perturbations.

The change of the E/I profile during cycling is explained through a complex reaction sequence which is in agreement with recently postulated reaction schemes and reported optical data.

INTRODUCTION

THE COMPLETE electrochemical characteristics of the anodic dissolution of nickel in aqueous sulphuric acid solutions using stationary and transient techniques have been studied over a long period of time by a large number of authors. The most relevant contributions made on the subject have been chosen from a great number of publications and have been chronologically quoted.[1–126] The possible explanations put forward for the existence of more than one current peak related to the electrodissolution of nickel as Ni(II) are neither coincident nor fully substantiated. The complex E/I characteristics obtained under linear potential sweep conditions at a constant temperature depend on the electrode history, the sequence and characteristics of the potential perturbation applied to the electrochemical interface, and the solution composition. The influence of the latter, however, is to some extent obscure owing to the fact that as the perturbation conditions are arbitrarily changed the experimental data are far from comparable. This is actually the case concerning the participation of sulphate ions in the kinetics of the anodic dissolution and passivation of nickel in acid electrolytes.[67,89,90]

The anodic current peaks recorded in the potential range where the anodic dissolution of nickel takes place were interpreted in terms of the formation of $Ni(OH)_2$ species.[33,36,52,99,121,122] The formation of $Ni(OH)_2$ corresponds to the first stage in the passivation of the metal which is actually completed when a Ni_2O_3-type species is formed at potentials more positive than those where the $Ni(OH)_2$ species exists.

Previous potentiodynamic studies revealed that the electrochemistry of the Ni/H_2SO_4 (aq) interface could be more complex than thought earlier.[115,120,121] The aim of the present paper is to extend previous studies made on the subject in an

*Manuscript received 29 April 1979; in revised form 19 July 1979.

attempt to obtain further information about the genesis and changing characteristics of the potentiodynamic E/I displays of the Ni/H_2SO_4 (aq) interface, mainly in the potential region where $Ni(OH)_2$ species are formed. It is also an attempt to derive more reliable quantitative kinetic data for the electrochemical reaction through the systematic change of the potential perturbation conditions.

EXPERIMENTAL METHOD

The experimental arrangement regarding the three compartment electrolysis cell, the electrodes, the chemicals employed and the solution preparation, were the same as those already reported in previous publications.[121,127,128] Specpure polycrystalline nickel working electrodes (Johnson, Matthey Ltd.) in the form of fixed wires without any special mechanical or thermal treatment (0.5 mm dia., 0.25 cm^2) were used. Three different electrode pretreatments were employed: (1) fine grade alumina polishing with a water–acetone–alumina suspension, (2) cathodization in a 0.1 N H_2SO_4 + 0.2 g/l thio-urea solution at 20 mA/cm^2 for 18 h at 25°C, to saturate the metal surface with electrolytic hydrogen, and (3) electropolishing for 2 min in 57% H_2SO_4. The potential of the working electrode was measured against a saturated calomel electrode and referred to the NHE scale.

The potential of the Ni/0.5 N H_2SO_4 interface at 25°C under 1atm. pressure nitrogen gas saturation was altered according to one of the programmes depicted in Fig. 1.[129] It consists of: (1) a repetitive triangular potential sweep, RTPS; (2) an intermediate potentiostatic ageing included during the repetitive potential sweeps (Figs. 1a and b); (3) an intermediate potentiodynamic ageing during the repetitive potential sweeps (Fig. 1c); and (4) a triangular-modulated triangular potential sweep, TMTPS (Fig. 1d).

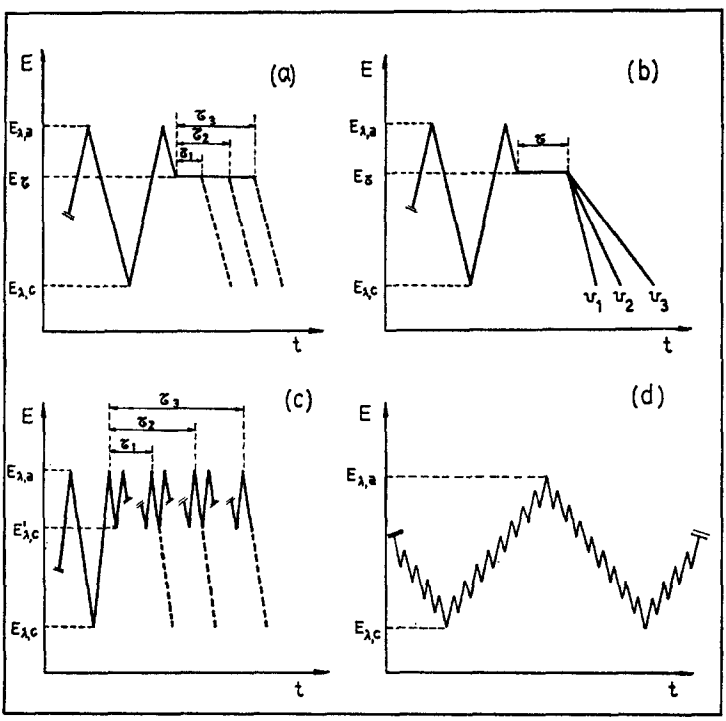

FIG. 1. Types of potential–time perturbation programmes employed in the present work.

EXPERIMENTAL RESULTS

The stabilized potential/current (E/I) profile which results after *ca.* 60 potential cycles is used as a reference. The number to attain the stabilized E/I display depends both on the potential sweep rate (v) and on the cathodic and anodic switching potentials ($E_{\lambda,c}$ and $E_{\lambda,a}$).

The stabilized E/I contours are, in principle, independent of the electrode pretreatment. The stabilized E/I profile at 0.1 V/s run between −0.26 and 0.54 V (Fig. 2b) exhibit during the anodic excursion two anodic current peaks, the larger one at *ca.* 0.2 V (Peak I) and the smaller one in the 0.3–0.4 V range (Peak II). The latter, however, depending on the perturbation conditions, may appear as a current plateau instead of a current peak. During the negative going potential scan, a small cathodic current peak at *ca.* −0.15 V is observed (Peak III) in the potential region just preceding the hydrogen evolution potential.

The influence of $E_{\lambda,a}$ on the genesis of Peak I during cycling (Fig. 2a) is similar to that previously encountered for aqueous H_2SO_4 solutions containing a large excess of $NiSO_4$.[115,121]

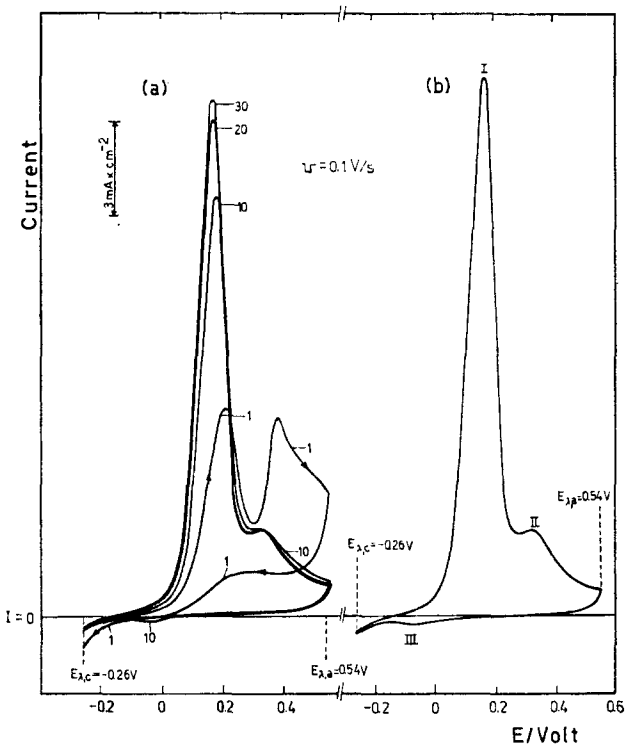

FIG. 2. Potentiodynamic E/I curves run with RTPS at 0.1 V/s. (a) Influence of the potential cycling on the E/I contours obtained from $E_{\lambda,c} = -0.26$ V to $E_{\lambda,a} = 0.54$ V. (b) Stabilized E/I profile.

The shape of the E/I displays recorded under the RTPS exhibit a remarkable dependence on $E_{\lambda,c}$ and $E_{\lambda,a}$ (Figs. 3 and 4). Thus, at 0.2 V/s when $E_{\lambda,c} = -0.26$ V (Fig. 3), as $E_{\lambda,a}$ decreases from 0.54 V to 0.34 V, i.e. to the potential where only

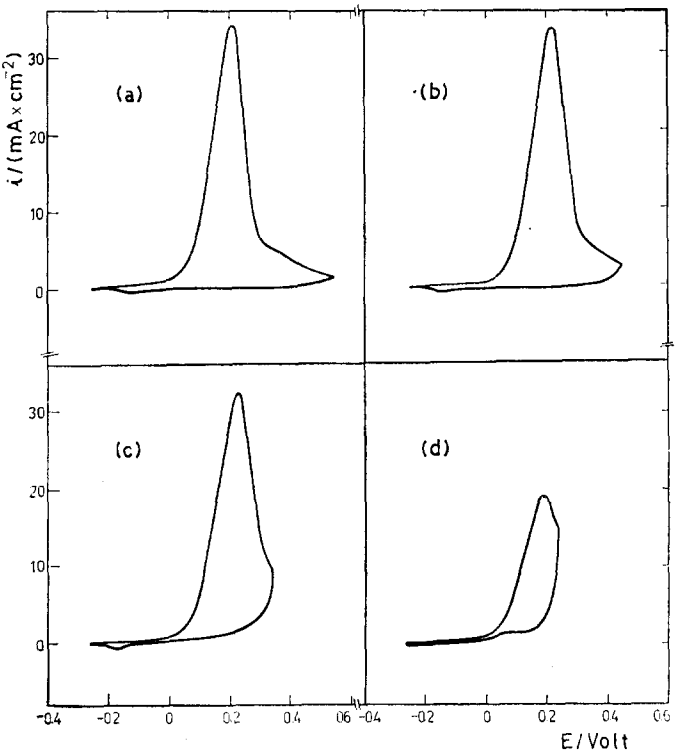

FIG. 3. Influence of the $E_{\lambda,a}$ on the stabilized RTPS E/I displays at 0.2 V/s and $E_{\lambda,c} = -0.26$ V. (a) $E_{\lambda,a} = 0.54$ V; (b) $E_{\lambda,a} = 0.44$ V; (c) $E_{\lambda,a} = 0.34$ V; (d) $E_{\lambda,a} = 0.24$ V.

Peak I is observed, the location of Peak III remains unchanged. But with a further decrease of $E_{\lambda,a}$ to a potential value slightly larger than the potential of Peak I such as 0.24 V, practically no contribution of Peak III is found. Furthermore, under these circumstances the negative direction potential excursion shows an anodic current plateau at potentials slightly more negative than those covered by Peak I. This effect is more noticeable as v decreases. Moreover, the anodic current contribution during the negative going potential scan increases as $E_{\lambda,a}$ decreases. On the other hand, when $E_{\lambda,a}$ is fixed at 0.54 V the progressive increase of $E_{\lambda,c}$ from *ca.* -0.36 to -0.16 V is accompanied by a systematic decreases of Peak I (Fig. 4). During the negative-going potential scan, Peak III is recorded only when $E_{\lambda,c} \leq -0.16$ V. The heights of Peaks I and II are nearly equal when $E_{\lambda,c} = -0.06$ V. But when $E_{\lambda,c} \leq -0.1$ V and $0.45 \text{ V} \leq E_{\lambda,a} \leq 0.6$ V ($I_{p,II}/I_{p,I}$), the height ratio of Peaks II and I, is 0.14 ± 0.015, a figure which is apparently independent of v in the $0.01 \text{ V/s} \leq v \leq 0.30$ V/s range.

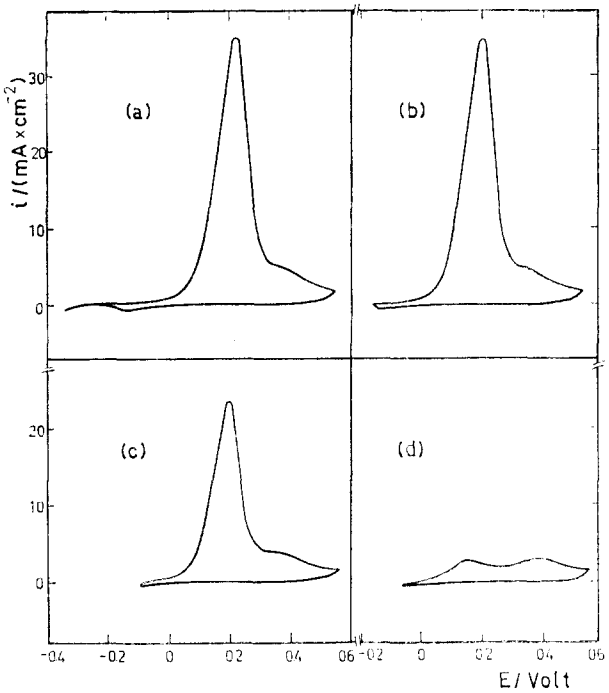

FIG. 4. Influence of the $E_{\lambda,c}$ on the stabilized RTPS E/I displays at 0.2 V/s and $E_{\lambda,a}$ = 0.54 V. (a) $E_{\lambda,c}$ = − 0.36 V; (b) $E_{\lambda,c}$ = − 0.26 V; (c) $E_{\lambda,c}$ = − 0.11 V; (d) $E_{\lambda,c}$ = − 0.06 V.

With both v and $E_{\lambda,a}$ constant, the potential of Peak I resulting during the potential cycling shifts towards more negative potentials as $E_{\lambda,c}$ becomes more positive. At constant v and $E_{\lambda,c}$, but with $E_{\lambda,c} \leq -0.3$ V, the potentials at which the null current is recorded both in the positive going and negative going potential excursions are different. However, their values are independent of $E_{\lambda,a}$ for $E_{\lambda,a} > 0.45$ V. Contrarily, when $E_{\lambda,c} > -0.1$ V, the $I_{p,II}/I_{p,I}$ ratio increases, the greater the rate of increase of the latter, the greater is the v value. Under these circumstances the stabilized E/I profile shows a much flatter Peak I and its potential is located at more negative values as $E_{\lambda,c}$ becomes progressively more positive.

The influence of v on the height and location of the various current peaks resulting from the stabilized RTPS run between $E_{\lambda,c} = -0.36$ V and $E_{\lambda,a} = 0.54$ V is depicted in Fig. 5. From this type of experiment reproducible and comparable kinetic parameters are derived (Table 1). Unfortunately as Peak III is poorly defined at low v_c, its dependence on v can only be derived when the cathodic reaction proceeds at a much larger potential sweep rate than that of the anodic reaction ($v_c > v_a$). At constant v and $E_{\lambda,c} \leq -0.3$ V the stabilized anodic profile becomes independent of either $E_{\lambda,c}$ or $E_{\lambda,a}$. Under these circumstances if $E_{\lambda,a}$ exceeds the potential range of Peak I, the charge of Peak III results in the order of one monolayer of the $Ni(OH)_2$ species on the nickel surface assuming an electrode roughness factor equal to one.

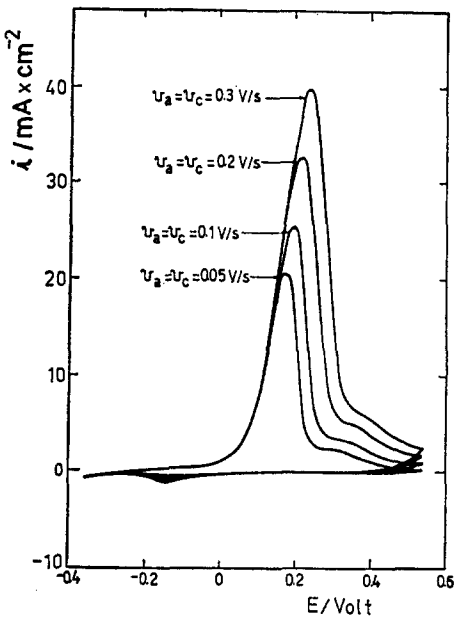

FIG. 5. Influence of the potential sweep rate on the stabilized potentiodynamic RTPS E/I displays recorded in the -0.36 to 0.54 V potential range.

TABLE 1. KINETIC PARAMETERS DERIVED FROM THE STABILIZED E/I DISPLAYS AS INDICATED IN THE TEXT.

$(\partial E_{p,I}/\partial \log v)$	$= 0.062 \pm 0.006$ V
$(\partial \log I_{p,I}/\partial \log v)$	$= 0.50 \pm 0.05$
$(\partial \log I_{p,II}/\partial \log v)$	$= 0.46 \pm 0.05$
$(\partial \log I_{p,III}/\partial \log v_c)_{v_a}$	$= 0.94 \pm 0.10$
$(\partial E_{p,III}/\partial \log v_c)_{v_a}$	$= 0.093 \pm 0.008$ V

The $E/\log I$ plots obtained from the ascending branch of Peak I, from the RTPS E/I profiles, fit reasonable straight lines with slopes from 0.04 V/decade at low v to 0.120 V/decade at high v.

E/I *displays obtained with complex potential perturbation programmes*

The experimental data described further on was recorded by perturbing the interface with different complex perturbation programmes applied to the electrochemical interface once the stable E/I profile was achieved through RTPS. In the following figures the stabilized E/I profiles are depicted by full traces.

A more detailed description of Peak III can be obtained by holding the potential at a value E_τ (0.39 V and 0.34 V, respectively) after the conventional RTPS during the time τ ($0.5\ m \leq \tau \leq 5.0\ m$) (Figs. 6 and 7). At both E_τ values a net anodic current is recorded. Then, at $v = 0.2$ V/s Peak III is clearly defined and its potential shifts towards more positive values as τ increases. This potential shift is probably due to the increase of the cathodic current baseline as τ increases. After holding the potential at E_τ the negative potential direction E/I profile exhibits a net cathodic depolarization. As E_τ decreases the above described effect is less noticeable but Peak III is now preceded by a hump (Fig. 7).

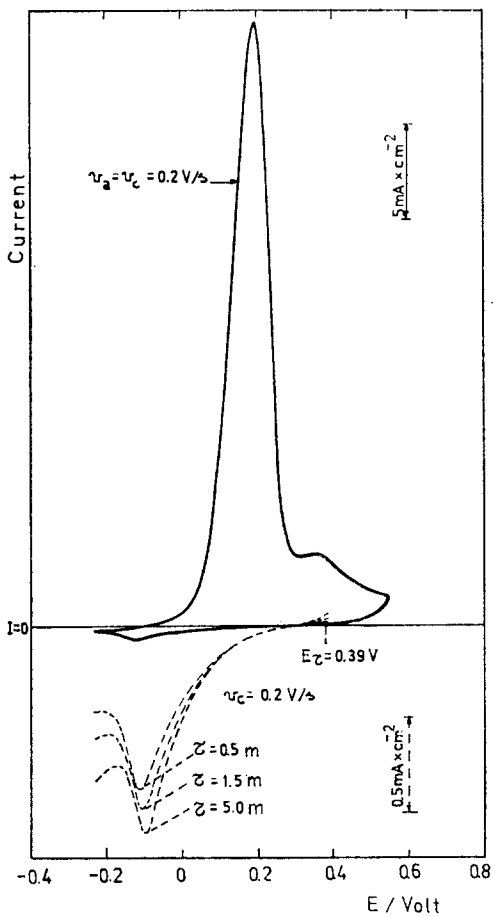

FIG. 6.

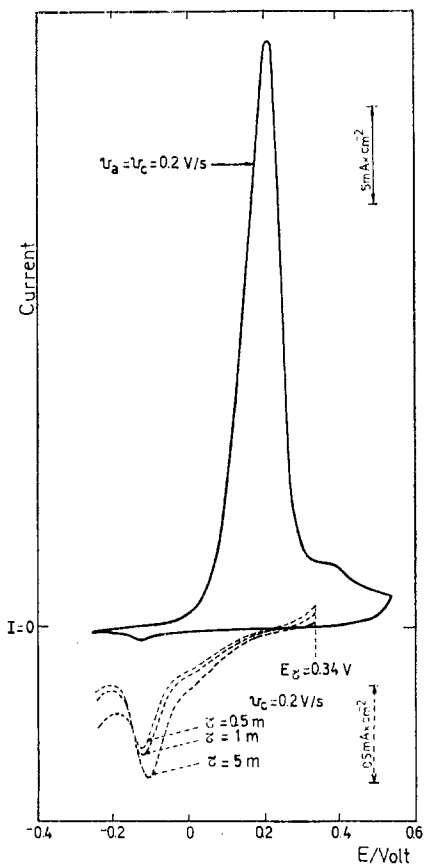

FIG. 7.

FIG. 6. Potentiodynamic E/I displays obtained with the perturbation programme of Fig. 1a at 0.2 V/s. The full trace is the stabilized RTPS E/I profile and the dashed traces correspond to negative going potential scans holding the potential at E_τ = 0.39 V during τ = 0.5, 1.5 and 5.0 min.

FIG. 7. Potentiodynamic E/I displays obtained with the perturbation programme of Fig. 1a at 0.2 V/s. E_τ = 0.24 V. τ = 0.5, 1.0 and 5.0 min.

Further details related to the E/I displays recorded during the negative going potential excursion at different v values result after holding the potential at E_τ (Figs. 8 and 9). Thus, for either $E_\tau = 0.34$ V or $E_\tau = 0.30$ V and $\tau = 1$ m, the E/I profile at the lower v values exhibits first an anodic current at more positive potentials and a cathodic current peak as the potential scan covers the more negative potential range. At the higher v values no anodic current is observed but there is a hump preceding the cathodic current peak. The effect is stronger as E_τ decreases, a fact which seems

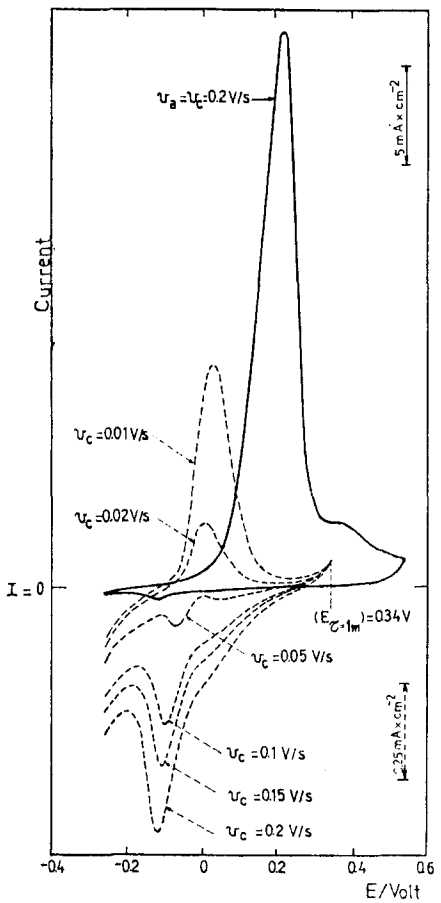

FIG. 8.

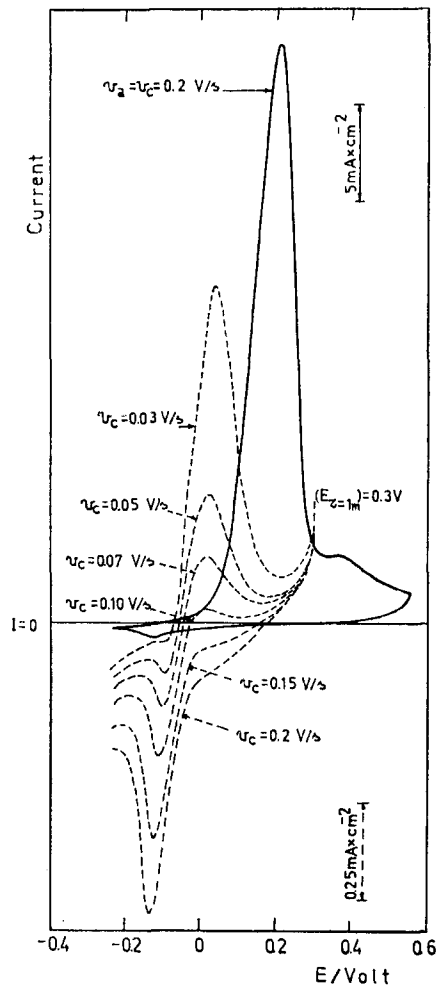

FIG. 9.

FIG. 8. Potentiodynamic E/I displays obtained with the perturbation programme of Fig. 1b. The full trace is the stabilized RTPS E/I profile at 0.2 V/s and the dashed traces correspond the negative going potential scans at 0.01, 0.02, 0.05, 0.10, 0.15 and 0.20 V/s after holding the potential at $E_\tau = 0.34$ V during $\tau = 1$ min.

FIG. 9. Potentiodynamic E/I displays obtained with the perturbation programme of Fig. 1b. The full trace is the stabilized RTPS E/I profile at 0.2 V/s and the dashed traces correspond to the negative going potential scans at 0.03, 0.05, 0.07 and 0.10 V/s after holding the potential at $E_\tau = 0.30$ V during $\tau = 1$ min.

to be related to the magnitude of the anodic current at E_τ. The anodic charge involved during the negative-going potential excursion is approximately equal to that required to passivate the electrode at more positive potentials. The slower the potential sweep rate, the greater the amount of the dissolving passivating species and, as a consequence, the anodic charge that participates during the cathodic excursion after holding the potential at E_τ becomes greater. The result is even more dramatic when E_τ decreases to either 0.24 or 0.19 V (Figs. 10 and 11). For $\tau = 1\ m$ (Fig. 10) after holding the

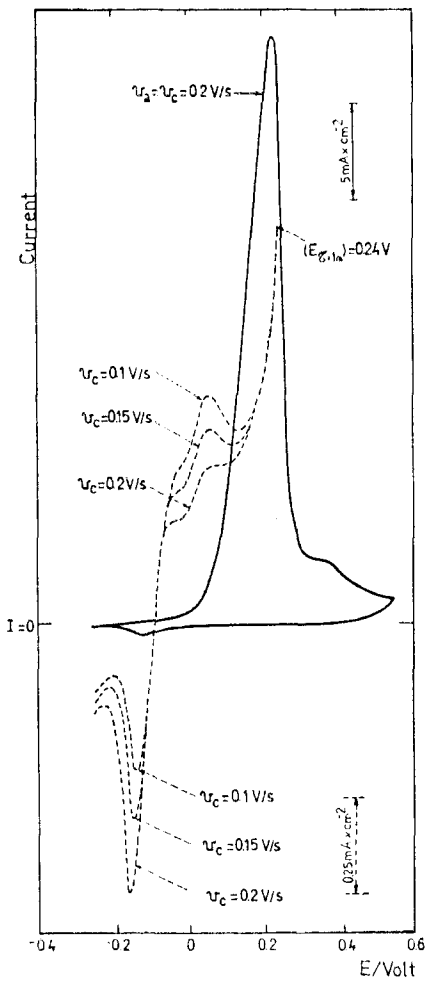

FIG. 10.

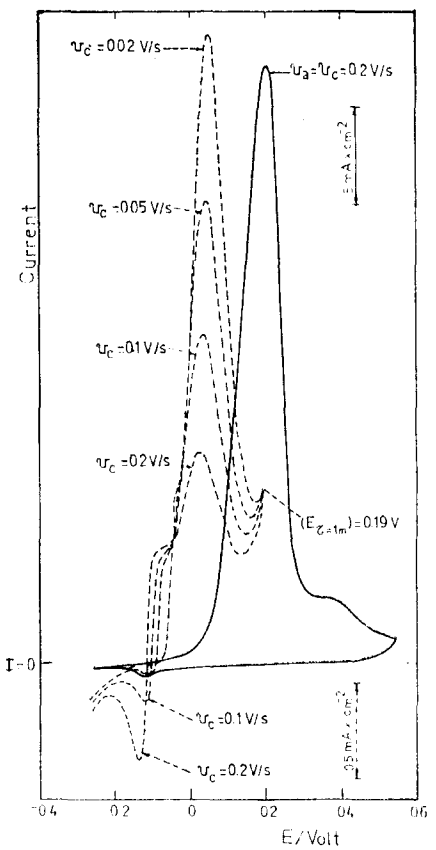

FIG. 11.

FIG. 10. Potentiodynamic *E*/*I* displays obtained with the perturbation programme of Fig. 1b. The full trace is the stabilized RTPT *E*/*I* profile at 0.2 V/s and the dashed traces correspond to the negative going potential scans at 0.10, 0.15 and 0.20 V/s after holding the potential at $E_\tau = 0.24$ V during $\tau = 1$ min.

FIG. 11. Potentiodynamic *E*/*I* displays obtained with the perturbation programme of Fig. 1b. The full trace is the stabilized RTPS *E*/*I* profile at 0.2 V/s and the dashed traces correspond to the negative going potential scans at 0.02, 0.05, 0.10 and 0.20 V/s after holding the potential at $E_\tau = 0.19$ V during $\tau = 1$ min.

potential at E_τ, the anodic current during the negative-going potential excursion presents the already described anodic current peak followed by an anodic current plateau. With $E_\tau = 0.19$ V, $\tau = 1\ m$ and different v values, a large contribution of the anodic charge during the cathodic excursion prevails at the lower potential sweep rates. As E_τ decreases the above mentioned anodic current contribution requires a larger v in order to retain the same magnitude.

The complexity of the anodic E/I contour after holding the potential at $E_\tau = 0.19$ V is clearly revealed by using different τ values (Fig. 12). Thus, for $\tau = 5\ m$ the occur-

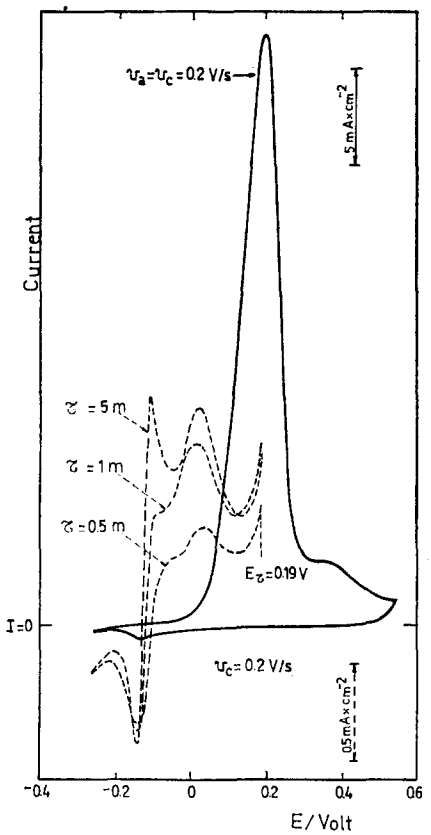

FIG. 12. Potentiodynamic E/I displays obtained with the perturbation programme of Fig. 1a at 0.2 V/s. $E_\tau = 0.19$ V. $\tau = 0.5$, 1.0 and 5.0 min.

rence of two anodic current peaks is established. The characteristics of the anodic E/I display can be systematically disclosed after perturbing the interface with the complex programme depicted in Fig. 13. Thus, the $I_{p,II}/I_{p,I}$ ratio increases with the time τ ($1\ m \leq \tau \leq 5\ m$) at $E_\tau = 0.04$ V but the overall anodic charge involved in the different E/I profiles remains practically constant. This apparently indicates that either an inter-conversion or an intraconversion of the passivating species occurs while the potential is held at E_τ. Contrarily, under the present circumstances no particular changes of the cathodic potential excursion E/I display are noticed when compared to those described above.

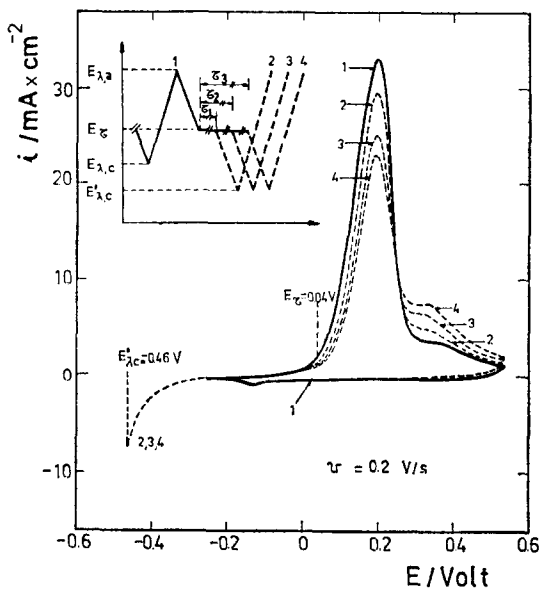

FIG. 13. Potentiodynamic E/I profiles run at 0.2 V/s with the perturbation programme shown in the figure. The full trace (curve 1) corresponds to the stabilized RTPS E/I display obtained between $-$ 0.26 and 0.54 V. The dashed traces correspond to the E/I curves recorded after holding the potential at E_τ during different times τ, from E_τ = 0.04 V up to $E'_{\lambda,c}$ = $-$ 0.46 V and backwards to $E_{\lambda,a}$ = 0.54 V. τ = 1 min (curve 2); τ = 3 min (curve 3); τ = 5 min (curve 4).

After applying the potentiodynamic ageing perturbation technique during $\tau = 1\ m$ (Fig. 14) (E/I profile No. 2), the potential sweep run towards the positive potential side immediately after the dynamic perturbation, presents a new anodic current peak (Peak IV) at *ca.* 0.9 V as shown in the Figure for three distinct anodic switching potentials. Furthermore, during the negative going potential excursion, Peak III is only observed when $E_{\lambda,a}$ is lower than the potential of Peak IV. The former shifts towards more negative potentials as $E_{\lambda,a}$ increases. Concomitantly, the depolarization of the hydrogen evolution reaction after the dynamic ageing is also evident. The effect is more remarkable when $E_{\lambda,a}$ extends towards more positive potentials although presumably a limiting $E_{\lambda,a}$ value should be involved.

The definition of the negative-going potential E/I profile is improved by running the E/I display at a constant v_a but different v_c (0.5 V/s $\leq v_c \leq$ 5 V/s) with an electrode which has been previously cathodically polarized for 1 min at $-$0.46 V and then stabilized with RTPS at 0.5 V/s between $-$0.46 V and 0.54 V under continuous stirring (Fig. 15). Thus, Peak III as well as the preceding cathodic current contribution become more clearly defined as v_c increases. Simultaneously, the corresponding current peak potential is more negative. The potential of Peak III is apparently independent of v_a and also of the switching potential values. However, the preceding current which appears as a shoulder on the positive side of Peak III, is well distinguished by 0.44 V $\leq E_{\lambda,a} \leq$ 0.94 V. The shoulder is located at more negative potentials when $E_{\lambda,a}$ increases, its contribution apparently overlaps with that of Peak III.

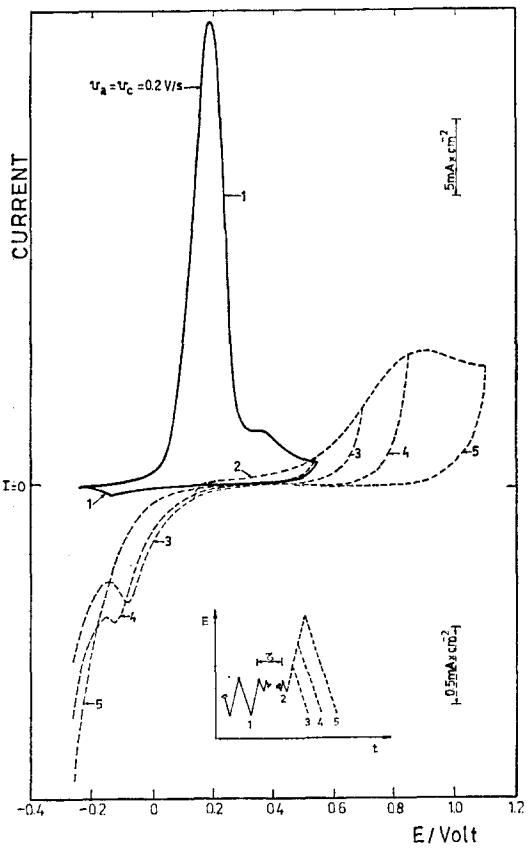

FIG. 14. Potentiodynamic E/I profiles run at 0.2 V/s with the E/t programme depicted in the figure. The full trace (curve 1) corresponds to the stabilized RTPS E/I display obtained between − 0.26 and 0.54 V. The number of the dashed traces correspond to those shown in the E/t perturbation programme.

The E/I records obtained under a TMTPS perturbation with modulating signal amplitudes (ΔE_m) lower than 0.06 V covering from $E_{\lambda,c} = -0.36$ V and $E_{\lambda,a} = 0.64$ V allows the distinction of the corresponding conjugated couples and their degree of reversibility in the potential range of Peaks I, II and III (Fig. 16). The E/I displays shown in the figures are comparatively depicted with the conventional RTPS E/I displays. The positive potential going E/I envelopes exhibit a relatively reversible conjugated couple in the *ca.* −0.15–0.05 V potential range in accordance to those obtained under RTPS at $v > 10$ V/s. At potentials more positive than 0.05 V the electrochemical reaction behaves as a completely irreversible process. This result is also related to the Tafel behaviour of the ascending portion of Peak I. The negative potential going E/I envelope firstly involves practically a small anodic current in the 0.6––0.1 V range. Then, at more negative potentials the previously described redox couple is again noticed but now another cathodic current contribution with a current peak at −0.2 V is observed. In the latter potential range, two well distinguished

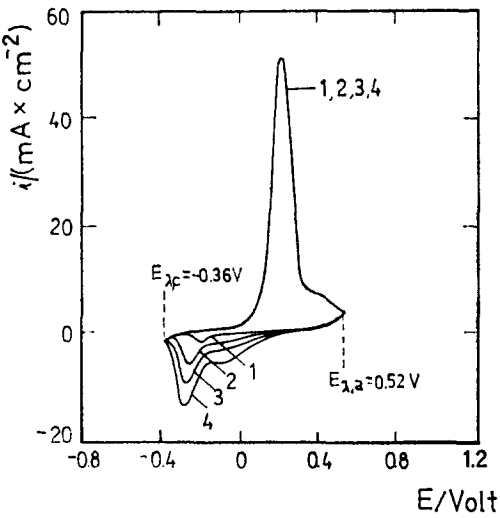

FIG. 15. Stabilized E/I displays recorded with asymmetric triangular potential sweeps between -0.36 and 0.52 V. $v_a = 0.5$ V/s. $v_c = 0.5$ V/s (1); $v_c = 2$ V/s (2); $v_c = 3$ V/s (3); $v_c = 5$ V/s (4).

conjugated redox couples are recorded when the base potential sweep is confined in the -0.26–0.24 V range (Figs. 17 and 18). However, the potentials of the current peaks corresponding to the conjugated redox couple recorded during the negative potential-going sweep shift a constant potential value towards more negative potentials than those of the redox couple recorded during the positive going potential sweep. When $E_{\lambda,a}$ is more negative than -0.1 V both redox couples are no longer observed. When the amplitude of the modulating signal exceeds 0.06 V, each modulating cycle always covers a potential range more extended than that of any single conjugated redox couple (Fig. 19). Therefore, the E/I contours are more complex, although the degree of reversibility of each process is well distinguished.

The reversible character of the redox couples is clearly defined when the frequency of the modulating signal (ν_m) is approx. 200 V/s and its amplitude is almost 0.06 V. This indicates that the rate constant of the electrochemical processes coupled with the potentiodynamic perturbation is of the order of 3×10^{-3} s^{-1}.

DISCUSSION

The potentiodynamic results pose two interesting problems related to the electrodissolution and first stage passivation of nickel. The first one is related to the change from the first E/I potentiodynamic record to those resulting in the so called stabilized E/I profiles resulting after a relatively large number of RTPS. The second problem is the possible explanation of the stabilized E/I profile. The sequence of E/I profiles depicted in Figs. 6–12 was obtained with systematic variation of the complex potentiodynamic perturbation program (Figs. 1a and b) ($0.19 \text{ V} \leq E_\tau \leq 0.39$ V; $0.5\ m \leq \tau \leq 5m$; 0.01 V/s $\leq v_c \leq 0.2$ V/s); they show dramatic changes in the E/I profiles in the neighborhood of E_r, the rest potential of the electrochemical interface, ($E_r \approx 0$ V).[121] These results are thus relevant to an understanding of the complexity of the initial

stages of nickel passivation in H_2SO_4 solution. This situation is even clearer when the stabilized *E/I* RTPS profiles (Figs. 3 and 4) are compared to those obtained in the same potential range, with the TMTPS perturbation (Figs. 16–19). These results can not be simply due to an effect associated with an increase of surface impurities as the potential is swept to progressively less positive potential limits.

In the acid solutions, the various anodic processes are occurring in the potential range where Peaks I and II are recorded. They are related to the electro-dissolution of the base metal and to the formation of passivating species. Within an appreciable large potential range both processes occur simultaneously. However, when one compares the kinetic results obtained in the Ni/0.5 N H_2SO_4 with those previously reported for the Ni/0.5 N H_2SO_4 + 1 N $NiSO_4$[121] one concludes that the anodic electrochemical process depends fundamentally on the solvent and acidity of the solution and only to a small extent on the SO_4^{2-} and Ni^{2+} ion concentrations. Therefore, the potentiodynamic characteristics of those interfaces at potentials more positive than the corresponding rest potentials are unlikely to be due to a precipitation and dissolution of $NiSO_4$ at the reaction interface.

The main difference between the first *E/I* display and those following is the systematic change of the *E/I* profile from the initial one, with the prevalence of Peak II, to another one involving after the *n*th cycle, the gradual increase of Peak I as the main current contribution. The change of the *E/I* profile corresponds to an increasing activation of the anodic reaction at the lower potentials. The gradual change of the *E/I* display is accompanied with an appreciable increase of the overall anodic charge taking place within the fixed switching potentials. At first sight the change of the electrode roughness may help to contribute to the charge increase. Nevertheless, the fact that there is a net and significant anodic charge during the RTPS, indicates that the main electrode reaction is

$$Ni = Ni^{2+} + 2\,e \tag{1}$$

which occurs through a complex reaction path, where various surface species are involved.

It is reasonable to assume that the first anodic potential cycle involves a Ni surface which is covered mostly by H_2O and to a lesser extent with adsorbed ions, approaching the equilibrium structure of the electrochemical double layer at the rest potential. Therefore, it is reasonable to interpret the electrodissolution of the metal formally through a modification of known mechanism[33,36] as follows:

$$Ni_x\,Ni(H_2O) = Ni_x\,Ni(OH) + H^+ + e \tag{2}$$

$$Ni_x\,Ni(OH) = Ni_x\,Ni(OH)^+ + e \tag{3}$$

$$Ni_x\,Ni(OH)^+ + H^+ = Ni^{2+} + Ni_{(x-1)}\,Ni(H_2O) \tag{4}$$

$$Ni_x\,Ni(OH)^+ + H_2O = Ni_x\,[Ni(OH)_2] + H^+ \tag{5}$$

$$Ni_x\,[Ni(OH)_2] = Ni_x + Ni^{2+} + 2\,OH^- \tag{6}$$

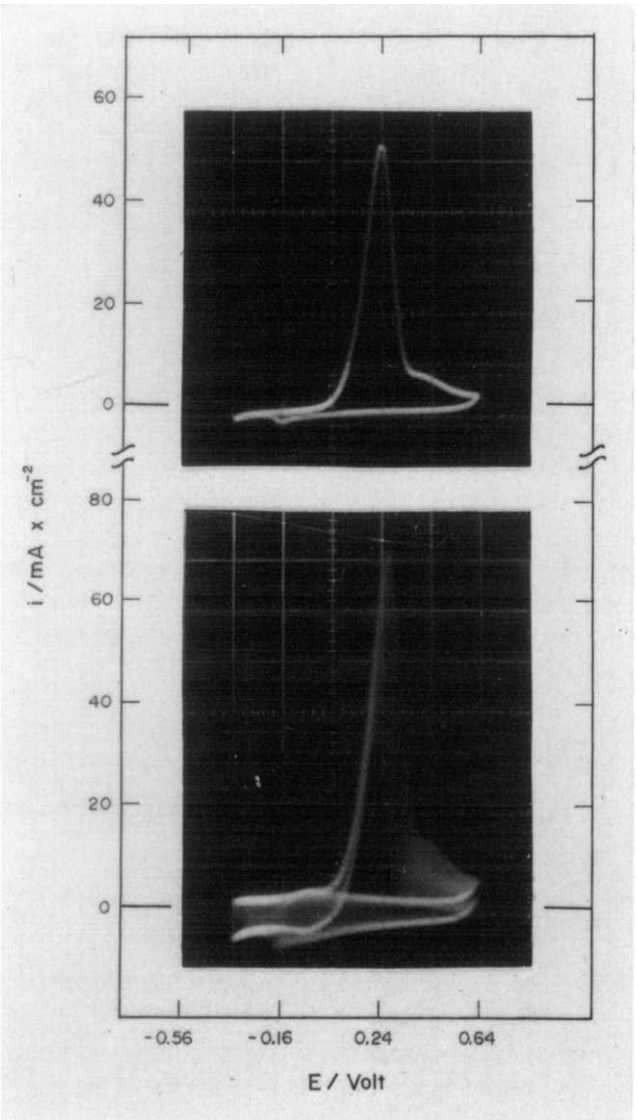

FIG. 16. Comparison between RTPS and TMTPS E/I displays run between $E_{\lambda,c}$ = 0.36 V and $E_{\lambda,a}$ = 0.64 V: (a) v = 0.5 V/s; (b) v_b = 0.5 V/s, v_m = 90 V/s, ΔE_m = 0.06 V.

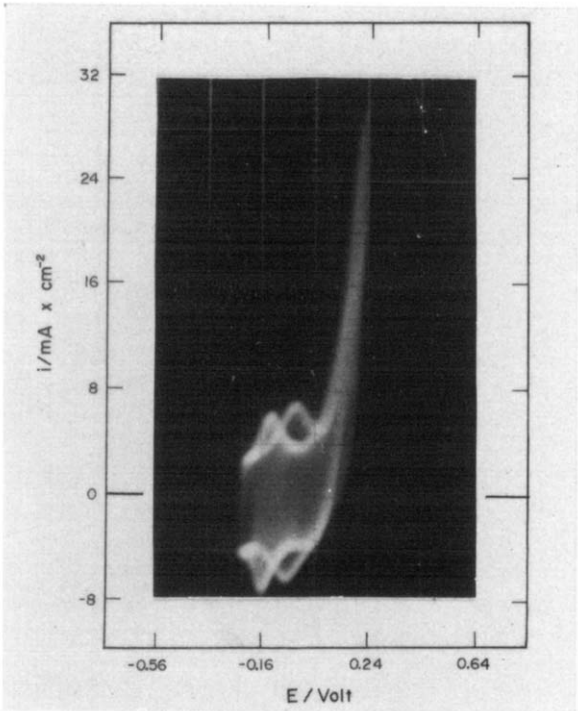

FIG. 17. E/I profile run with TMTPS between $E_{\lambda,c} = -0.26$ V and $E_{\lambda,a} = 0.24$ V. $v_b = 0.5$ V/s, $v_m = 90$ V/s, $\Delta E_m = 0.06$ V.

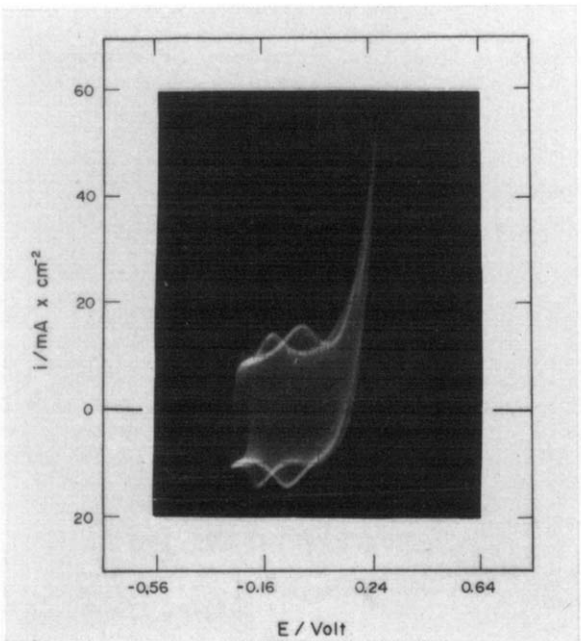

FIG. 18. E/I profile run with TMTPS between $E_{\lambda,c} = -0.26$ V and $E_{\lambda,a} = 0.24$ V. $v_b = 5$ V/s, $v_m = 200$ V/s, $\Delta E_m = 0.06$ V.

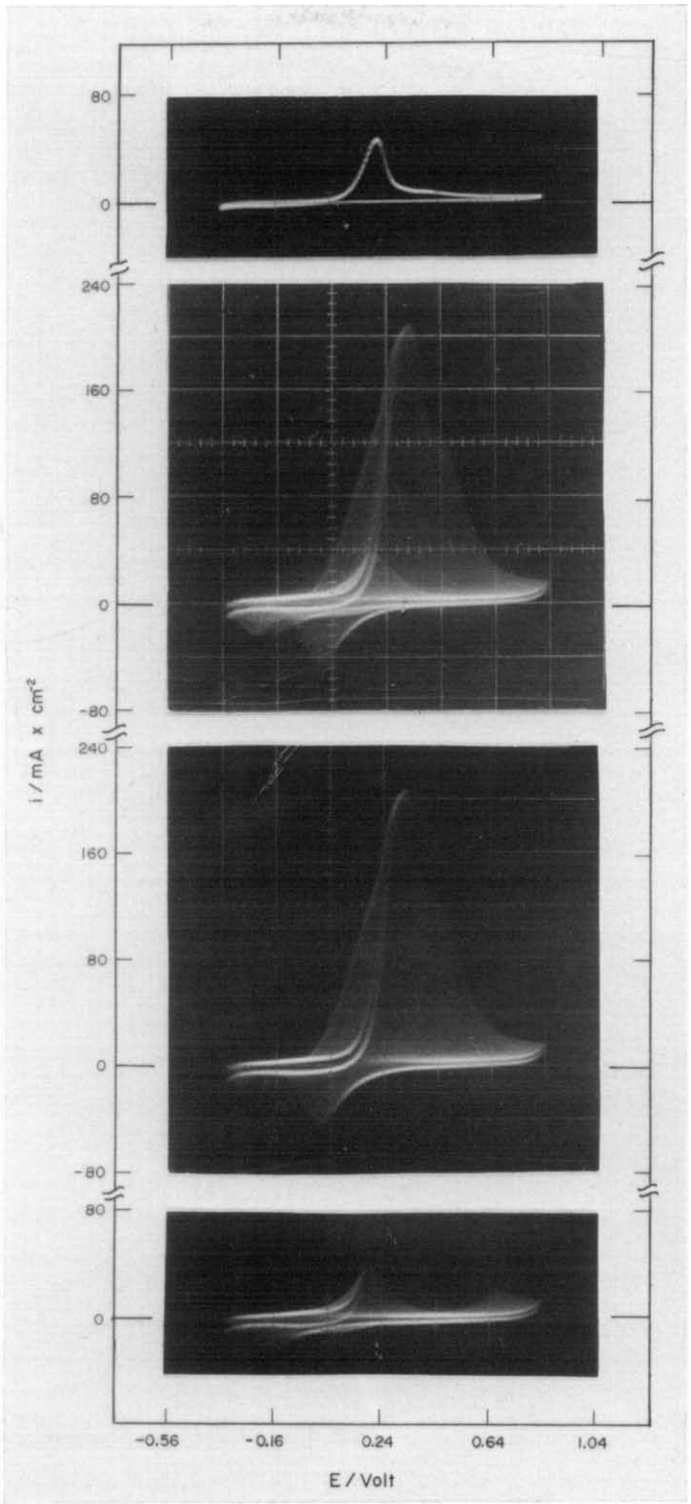

FIG. 19. Comparison between RTPS and TMTPS voltammograms run between $E_{\lambda,c} = -0.36$ V and $E_{\lambda,a} = 0.84$ V. (a) $v = 0.5$ V/s; (b) $v_b = 0.5$ V/s, $v_m = 90$ V/s, $\Delta E_m = 0.42$ V; (c) positive potential going E/I contour corresponding to the display (b); (d) negative potential going E/I contour corresponding to the display (b). For the latter the initial portion of the negative going potential E/I contour is distorted by the partial overlapping of the preceding positive potential sweep.

$$Ni_{(x-1)}\{2[Ni(OH)_2]\} = Ni_{(x-1)}[(NiOOH) \cdot Ni(OH)_2] + H^+ + e \quad (7)$$

where Ni_x denotes the bulk metal, the parenthesis and the brackets refer to adsorbed surface species and to film forming species, respectively. Steps (2–4), involving step (3) as rate-determining, correspond to the usually accepted mechanism for the active dissolution of nickel in acid electrolytes.[26,36,98,112,121] Step (5), occurring in parallel, shows the formation of a nickel hydroxide-type layer on the electrode. The latter species, which dissolves chemically through step (6) is apparently responsible for the anodic passivation related to Peak II. Step (7) takes place at high positive potentials.

During the RTPS, the situation at the interface should become appreciably different. If the anodic potential sweep is fast enough to avoid either the chemical dissolution of the film anodically formed or to exceed the time to establish the water re-adsorption equilibria, then the electrode surface related to the initiation of each positive-going excursion is represented by the average composition $Ni_x\ Ni(OH)_2$. Thus, the new initial surface structure consists of a film-covered electrode surface which assists the electro-dissolution process. Therefore, the corresponding sequence of reactions can be put forward as follows:

$$Ni_x[Ni(OH)_2] + H_2O = Ni_x[Ni(OH)_2 \cdot H_2O] \quad (8)$$

$$Ni_x[Ni(OH)_2 \cdot H_2O] = Ni_{(x-2)}[3\ (NiOH)] + H^+ + e \quad (9)$$

$$Ni_{(x-2)}[3\ (NiOH)] = Ni_{(x-2)}[2\ (NiOH) \cdot NiOH^+] + e \quad (10)$$

$$Ni_{(x-2)}[2\ NiOH.NiOH^+] + H^+ = Ni_{(x-1)}[Ni(OH)_2] + Ni^{2+} + H_2O \quad (11)$$

The reaction sequence (8–11) is associated with the characteristics of the stabilized RTPS *E/I* profile (Figs. 3–5). Therefore, under the usual stationary metal electro-dissolution conditions both reaction mechanisms contribute to the overall reaction.

According to the preceding reaction pathways the $Ni(OH)_2$ species causes the first stage of passivation. The latter process competes with the chemical dissolution of the $Ni(OH)_2$ species. Therefore, the potential for the occurrence of the maximum current should depend on the degree of participation of the various processes in the overall anodic reaction. The dependence of the anodic current peak and of its charge on the potential perturbation conditions including $E_{\lambda,a}$ and $E_{\lambda,c}$ indicate that the first stage passivation mechanism is predominantly a precipitation-dissolution mechanism, instead of a pure activation controlled film forming mechanism. This conclusion is confirmed by the square root dependence of the height of current peaks I and II on the potential sweep rate and on the stirring conditions prevailing at the reaction interface. This explains why when $E_{\lambda,a} < ca.\ 0.4$ V, the negative-going potential excursion exhibits an anodic current contribution whose charge complements the charge of the preceding positive-going excursion necessary to achieve the electrode passive state. It is also clear that the passivating species produced at $E_{\lambda,a} < 0.4$ V is easily electroreduced at potentials more negative than -0.1 V.

From the present results (Fig. 14) there is clear evidence that at $E_{\lambda,a} > 0.4$ V a new passivating species is produced. Taking into account that in the potential range

exceeding 0.4 V the formation of Ni(III) species is thermodynamically possible, the following electrochemical reaction becomes feasible:

$$Ni_x\,[Ni(OH)_2] = Ni_{(x-2)}\,[Ni(OH)_2 \,.\, NiOOH] + H^+ + e \qquad (12)$$

and, consequently, the complementary electrodissolution reaction then occurs through an interface containing a mixture of at least the two non-equilibrated passivating species.

The existence of the various OH-containing surface species as well as their possible chemical interconversion and dissolution, can be deduced from the negative-going potential excursion recorded after holding the potential at different values. There are qualitative suggestions in the literature that oxide films formed on anodized nickel in acid solutions are also susceptible to electro-reduction in these acid solutions. However, only very recently quantitative information has been reported on either determining the extent of oxide removal at various pH values or in characterizing the nickel oxides species formed at the electrochemical interface. The number of cathodic current contributions and the overall shape of the E/I contour during the negative-going potential excursion depends both on $E_{\lambda,a}$ and on v (Fig. 15). Thus, when $E_{\lambda,a} \leq 0.3$ V, that is in the potential range of Peak I, unless v exceeds 0.05 V/s practically only one single cathodic current contribution characterized by a current peak at *ca.* −0.15 V is seen. The fact that the latter current peak is not observed when $v < 0.05$ V/s, under the conditions shown in Fig. 9, demonstrates that the $Ni(OH)_2$ passivating species easily dissolves in the acid electrolyte. On the other hand, Peak III, at −0.15 V thereabouts, involves a charge of the order of one monolayer and corresponds to a process which occurs at the initiation of the hydrogen evolution reaction. The reversible characteristics of the conjugated couple related to this current peak is clearly revealed by the TMTPS experiments (Fig. 17). The fast conjugated redox couple should be assigned to the first electron transfer and de-protonation process which initiates either the reaction sequence (2–7) or (8–11). The initial reaction can be simply written

$$Ni + H_2O = NiOH + H^+ + e \qquad (13)$$

as formerly postulated to account for the anodic electro-dissolution of nickel in acid solutions.[26,36,121] However, the corresponding charge suggests that the condition of low coverage by the adsorbed intermediate, assumed in earlier mechanistic analysis of the anodic dissolution of nickel in acid electrolytes is apparently not fullfilled. The height of the cathodic current peak related to the electro-reduction of the NiOH surface species follows a first order dependence on v although no dependence of the cathodic current peak potential on v is observed. These results are in agreement with the simplest theory of potentiodynamic formation of a passivating monolayer according to a reversible single electron transfer step.[130]

When $E_{\lambda,a} > 0.3$ V, there is a new cathodic current contribution at *ca.* 0 V, which distorts the shape of Peak III. Apparently the species formed in the potential range of the Peak II, which was assigned to the $Ni(OH)_2$.NiOOH-type species, electroreduces in the 0.1 – −0.2 V range. The amount of products accumulated during the overall anodic process increases as the time τ at E_τ increases. From the comparison

of the time dependence of the cathodic E/I profile shown in Figs. 7 and 12, one can deduce that the rate of the chemical dissolution of the [$Ni(OH)_2$.NiOOH] species is lower than that of the Ni $(OH)_2$ species. An estimation of the relative dissolution rates comes from the cathodic potential sweep rate (v_c) required to cancel the anodic current contribution, when the potential excursion initiates from different $E_{\lambda,a}$ values. Thus, as $E_{\lambda,a}$ decreases, the value of v_c decreases, as the anodic passivating species dissolves faster. The dissolution rate of the $Ni(OH)_2$ species is about twice that of the [$Ni(OH)_2$.NiOOH] species. The second passivating species which is electrochemically produced from the first one according to reaction (6) (Fig. 13) is also very difficult for electroreducing. At 0.04 V, the species remains on the surface so that the surface available for the formation of the first passivating species is smaller as the time at 0.04 V increases.

The stability of the different species related to the various prepassive stages can be estimated by means of the potentiodynamic ageing technique[131] applied within the potential range of the corresponding electroformations (Fig. 14). One observes that after the rapid intermediate low amplitude RTPS, the following E/I display exhibits a small but net and broad anodic current peak at *ca.* 0.8 V which corresponds to the onset of complete passivity due to the [$Ni_2O_3.H_2O$] film formation according to:

$$Ni_x[Ni(OH)_2.NiOOH] \rightarrow Ni_x\,[2\ NiOOH] \xrightarrow[-\,(H^+ + e)]{} Ni_x\,[Ni_2O_3.H_2O] \qquad (14)$$

When the latter is formed the restoration of the initial electrode activity is only achieved after a cathodic polarization at potentials where a net H_2 discharge is produced.[115,121] The [Ni_2O_3] species represents the simplest way of indicating a NiO lattice involving hole formation of Ni(III) species into the lattice, as discussed previously.[120,121]

In conclusion, the present results can be summarized as follows. The anodic dissolution of Ni in the acid electrolyte involves a metal surface which is covered either partially or completely by one of the following species NiOH, $NiOH^+$, $Ni(OH)_2$ or [$Ni(OH)_2$.NiOOH]. These species are actually related to the initial stage passivation region of the E/I curves. The last two species may produce the formation of a new phase which is soluble in the acid electrolyte. Their dissolution competes with the metal electro-oxidation and phase rebuilding. The [$Ni(OH)_2$.NiOOH] species may continue its further electro-oxidation at higher positive potentials, yielding complete passivity through the formation of the [Ni_2O_3] species. The electro-reduction characteristics of those species not only confirm their existence but furnish more details about the initial stage passivation region of the Ni/H_2SO_4 interface.

Acknowledgement—INIFTA is sponsored by the Consejo Nacional de Investigaciones Cientificas y Técnicas, the Universidad Nacional de La Plata and the Comisión de Investigaciones Científicas (Provincia de Buenos Aires). This work was partially supported by the SENID (Navy Research and Development Service of Argentina) and the Regional Programme for the Scientific and Technological Development of the Organization of the American States.

REFERENCES

1. W. J. MÜLLER, *Z. Elektrochem.* **33**, 401 (1927).
2. D. R. TURNER, *J. electrochem. Soc.* **98**, 434 (1951).
3. YA. M. KOLOTYRKIN, *Z. Elektrochem.* **62**, 664 (1958).

4. K. SCHWABE and G. DIETZ, *Z. Elektrochem.* **62**, 751 (1958).
5. G. OKAMOTO, H. KOBAYASHI, M. NAGAYAMA and N. SATO, *Z. Elektrochem.* **62**, 775 (1958).
6. R. PIONTELLI and G. SERRAVALLE, *Z. Elektrochem.* **62**, 759 (1958).
7. G. OKAMOTO and N. SATO, *Trans. Japan Inst. Metal.* **1**, 16 (1960).
8. K. SCHWABE, *Electrochim. Acta* **3**, 186 (1960).
9. K. ARNOLD and K. J. VETTER, *Z. Elektrochem.* **64**, 244 (1960).
10. K. ARNOLD and K. J. VETTER, *Z. Elektrochem.* **64**, 407 (1960).
11. J. OSTERWALD and H. G. FELLER, *J. electrochem. Soc.* **107**, 473 (1960).
12. E. RAUB anc A. DISAM, *Metalloberfläche* **15**, 193 (1961).
13. E. RAUB and A. DISAM, *Metalloberfläche* **15**, 229 (1961).
14. G. ECONOMY, R. SPEISER, F. H. BECK and M. G. FONTANA, *J. electrochem. Soc.* **108**, 337 (1961).
15. J. OSTERWALD and H. H. UHLIG, *J. electrochem. Soc.* **108**, 505 (1961).
16. N. Y. BUNE and Y. M. KOLOTYRKIN, *Russ. J. phys. Chem.* **35**, 757 (1961).
17. L. F. TRUEB, G. TRUEMPLER and N. IBL, *Helv. Chim. Acta* **44**, 1433 (1961).
18. V. EBERSBACH, K. SCHWABE and K. RITTER, *Electrochim. Acta* **12**, 241 (1962).
19. N. D. GREENE, *First International Congress on Metallic Corrosion*, p. 113, London (1962).
20. J. L. WEININGER and M. W. BREITER, *J. electrochem. Soc.* **110**, 484 (1963).
21. N. SATO and G. OKAMOTO, *J. electrochem. Soc.* **110**, 605 (1963).
22. M. L. KRONENBERG, J. C. BANTER, E. YEAGER and F. HOVORKA, *J. electrochem. Soc.* **110**, 1007 (1963).
23. E. KUNZE and K. SCHWABE, *Corros. Sci.* **4**, 109 (1964).
24. M. KEDDAM and I. EPELBOIN, *C.R. Acad. Sci., Paris* **259**, 137 (1964).
25. A. K. HUG, A. ROSENBERG and A. C. MAKRIDES, *J. electrochem. Soc.* **111**, 278 (1964).
26. N. SATO and G. OKAMOTO, *J. electrochem. Soc.* **111**, 897 (1964).
27. T. ISHIKAWA and G. OKAMOTO, *Electrochim. Acta* **9**, 1259 (1964).
28. E. A. MICHAILOVA and Z. A. IOFA, *Elektrokhimiya* **1**, 89 (1965).
29. G. A. DI BARI and J. V. PETROCELLI *J. electrochem. Soc.* **112**, 99 (1965).
30. N. Y. BUNE, *Zashch. Met.* **1**, 168 (1965).
31. G. TRABANELLI, F. ZUCCHI and L. FELLONI, *Corros. Sci.* **5**, 211 (1965).
32. R. R. SAYANO and K. NOBE, Water Resources Center Contrib. 104; Report No. 65–38 (1965).
33. A. K. N. REDDY, M. G. B. RAO and J. O'M. BOCKRIS, *J. Chem. Phys.* **42**, 2246 (1965).
34. K. SCHWABE, *Angew. Chem.* **78**, 253 (1966).
35. T. S. DE GROMOBOY and L. L. SHREIR, *Electrochim. Acta* **11**, 895 (1966).
36. J. O'M. BOCKRIS, A. K. N. REDDY and B. RAO, *J. electrochem. Soc.* **113**, 1133 (1966).
37. I. A. AMMAR and S. DARWISH, *Electrochim. Acta* **11**, 1541 (1966).
38. M. DAGUENET, M. FROMENT and M. KEDDAM, *J. Microscopie* **5**, 569 (1966).
39. I. A. AMMAR and S. DARWISH, *Electrochim. Acta* **12**, 225 (1967).
40. J. POSTLETHWAITE and D. R. HURP, *Corros. Sci.* **7**, 435 (1967).
41. J. MIELUCH, *Bull. Acad. Polon. Sci., Sér. Sci. Chim.* **15**, 591 (1967).
42. K. SCHWABE, *Werkst. Korros.* **18**, 961 (1967).
43. Y. M. KOLOTYRKIN, *Zashch. Metal.* **3**, 131 (1967).
44. H. G. FELLER and J. RÜCKERT, *Z. Metallk.* **58**, 635 (1968).
45. I. A. AMMAR and S. DARWISH, *Electrochim. Acta* **13**, 781 (1968).
46. A. T. VAGRAMYAN, M. A. ZHAMAGORTSYAN, L. A. UVAROV and A. A. YAVICH, *Zashch. Metal.* **5**, 74 (1969).
47. F. OVARI and A. L. ROTINYAN, *Zh. Prikl. Khim.* **42**, 227 (1969).
48. G. GILLI, P. BOREA, F. ZUCCHI and G. TRABANELLI, *Corros. Sci.* **9**, 673 (1969).
49. U. EBERSBACH, K. SCHWABE and P. KOENIG, *Electrochim. Acta* **14**, 773 (1969).
50. A. S. VALEEV and A. M. USHANOVA, *Elektrokhimiya* **5**, 809 (1969).
51. L. N. YAGUPOLS'KAYA and B. A. MOUCHAN, *Proc. 4th Int. Congr. on Metal. Corrosion*, p. 473, Amsterdam (1969).
52. A. K. N. REDDY and B. RAO, *Can. J. Chem.* **47**, 2687 (1969).
53. A. M. SUKHOTIN and P. P. STANISHEVSKII, *Tr. Gos. Inst. Prikl. Khim.* **64**, 78 (1970).
54. A. B. IJZERMANS, *Corros. Sci.* **10**, 113 (1970).
55. F. OVARI and A. L. ROTINYAN, *Elektrokhimiya* **6**, 516 (1970).
56. K. NII, *Corros. Sci.* **10**, 571 (1970).
57. A. R. YAMUNA and N. SUBRAMANYAN, *Werkst. Korros.* **21**, 607 (1970).
58. A. T. VAGRAMYAN, M. A. ZHAMAGORTSYAN, L. A. UVAROV and A. A. YAVICH, *Elektrokhimiya* **6**, 733 (1970).
59. C. J. MAUVAIS, R. M. LATANISION and A. W. RUFF, *J. electrochem. Soc.* **117**, 902 (1970).
60. B. LOVRECEK and S. LIPANOVIĆ, *Corros. Sci.* **10**, 865 (1970).

61. A. I. OSHE and V. A. LOVACHEV, *Elektrokhimiya* **6**, 1416 (1970).
62. J. MIELUCH, Bull. Acad. Polon. Sci., *Sér. Sci. Chim.* **19**, 249 (1971).
63. I. GARZ and U. HÄFKE, *Corros. Sci.* **11**, 329 (1971).
64. R. M. LATANISION and H. OPPERHAUSER, *Corrosion* **27**, 509 (1971).
65. R. L. COWAN and R. W. STAEHLE, *J. electrochem. Soc.* **118**, 557 (1971).
66. R. D. ARMSTRONG, *Corros. Sci.* **11**, 693 (1971).
67. M. KESTEN and H. G. FELLER, *Electrochim. Acta* **16**, 761 (1971).
68. I. N. ANDREEV, I. M. NOVOSEL'SKII and M. G. KHAKIMOV, *Elektrokhimiya*, **7**, 1004 (1971).
69. A. I. OSHE, E. K. OSHE and I. L. ROZENFELD, *Elektrokhimiya* **7**, 1419 (1971).
70. G. BONDEAU, M. ROELICHER, M. FROMENT and A. HUGOT-LE GOFF, *C.R. Acad. Sci. Paris* **275**, 25 (1972).
71. J. SIEJKA, C. CHERKI and J. YAHALOM, *Electrochim. Acta* **17**, 161 (1972).
72. H. G. FELLER, H. J. RÄTZER-SCHEIBE and W. WENDT, *Electrochim. Acta* **17**, 187 (1972).
73. R. D. ARMSTRONG and M. HENDERSON, *J. Electroanal. Chem.* **39**, 222 (1972).
74. H. RÄTZER-SCHEIBE and H. G. FELLER, *Z. Metallkde.* **63**, 351 (1972).
75. U. EBERSBACH, G. KREYSA and K. SCHWABE, *Electrochim. Acta* **17**, 445 (1972).
76. C. J. CHATFIELD and L. L. SHREIR, *Corros. Sci.* **12**, 563 (1972).
77. H. G. FELLER, M. KESTEN and J. KRUPSKI, *Proc. 5th Int. Congr. Met. Corros.* p. 155 (1972).
78. A. C. HART and S. A. WATSON, *Galvano* **41**, 763 (1972).
79. K. SCHWABE, U. EBERSBACH and W. LEIMBROCK, *Electrochim. Acta* **17**, 957 (1972).
80. J. SIEJKA, C. CHERKI and J. YAHALOM, *J. electrochem. Soc.* **119**, 991 (1972).
81. G. N. TRUSOV and M. F. FANDEEVA, *Elektrokhimiya* **8**, 1008 (1972).
82. I. M. NOVOSEL'SKII, M. G. KHAKIMOV and M. SH. GIZATULLIN, *Elektrokhimiya* **8**, 1474 (1972).
83. V. S. BAGOTZKY, N. A. SHUMILOVA, G. P. SAMOILOV and E. I. KHRUSCHCHEVA, *Electrochim Acta* **17**, 1625 (1972).
84. I. M. NOVOSEL'SKII and M. G. KHAKIMOV, *Elektrokhimiya* **9**, 34 (1973); **9**, 38 (1973); **9**, 340 (1973); **9**, 484 (1973).
85. W. PAATSCH, *Surface Sci.* **37**, 59 (1973).
86. A. C. HART, *Trans. Inst. Metal Finish.* **51**, 69 (1973).
87. H. J. RÄTZER-SCHEIBE and H. G. FELLER, *Electrochim. Acta* **18**, 175 (1973).
88. C. R. CROWE and S. G. FISHMAN, *Corros. Sci.* **13**, 569 (1973).
89. YA. M. KOLOTYRKIN, YU. A. POPOV and YU. V. ALEKSEEV, *Elektrokhimiya* **9**, 624 (1973); **9**, 629 (1973).
90. N. A. BALASHOVA, N. T. GOROKHOVA and S. A. LILIN, *Elektrokhimiya*, **9**, 666 (1973).
91. I. A. GINDIN, L. N. YAGUPOL'SKAYA, W. K. AKSENOV and YA. D. STARODUBOV, *Corros. Sci.* **13**, 967 (1973).
92. M. TURNER, G. E. THOMPSON and P. A. BROOK, *Corros. Sci.* **13**, 985 (1973).
93. I. N. ANDREEV, N. SH. GIZATULLIN and V. E. ZUBAREVA, *Prikl. Elektrokhimiya* **3**, 25 (1974).
94. G. BONDEAU, M. FROELICHER, M. FROMENT and A. HUGOT-LE GOFF, *Phys. Stat. Sol.* **26**, 181 (1974).
95. L. TAMM, U. TAMM and V. PAST. *Tartu Riikliku Ulik. Toim.* **3**, 332 (1974).
96. A. PIGEAUD, *J. electrochem. Soc.* **122**, 80 (1975).
97. I. N. ANDREEV, O. N. TEREKHOVA and M. S. MISHCHENKO, *Tr. Kazan. Khim. Technol. Inst.* **56**, 86 (1975).
98. G. T. BURSTEIN and G. A. WRIGHT, *Electrochim. Acta* **20**, 95 (1975).
99. V. N. KOVTUN, V. F. MOGILENKO and A. M. GRESHIK, *Elektrokhimiya* **11**, 277 (1975).
100. L. N. YAGUPOL'SKAYA, *Zashch. Met.* **11**, 338 (1975).
101. B. MAC DOUGALL and M. COHEN, *J. electrochem. Soc.* **122**, 383 (1975).
102. M. A. ZHAMAGORTSYAN, Z. N. PILIKYAN and A. T. VAGRAMYAN, *Elektrokhimiya* **11**, 345 (1975).
103. O. G. DERIAGINA and E. N. PALEOLOG, *Elektrokhimiya* **11**, 1003 (1975).
104. N. SATO, *Boshoku Gijutsu* **25**, 35 (1976).
105. K. DEO, S. G. MEHENDALE and S. VENKATACHALAM, *J. appl. Electrochem.* **6**, 37 (1976).
106. D. ALTURA and K. NOBE, *Corrosion* **32**, 41 (1976).
107. J. P. PETITJEAN and H. VANDERPOORTEN, *Trait. Surf.* **17**, 43 (1976).
108. A. JOUANNEAU and M. C. PETIT, *J. Chim. Phys.* **73**, 82 (1976).
109. K. S. G. DOSS and D. DESHMUKH, *J. electroanal. Chem.* **70**, 141 (1976).
110. B. MACDOUGALL and M. COHEN, *J. electrochem. Soc.* **123**, 191 (1976).
111. A. JOUANNEAU, M. KEDDAM and M. C. PETIT, *Electrochim. Acta* **21**, 287 (1976).
112. D. W. JEFFERS and K. NOBE, *Corrosion* **32**, 438 (1976).
113. A. E. H. BRUESCHKE and H. K. ELBERT, *Werkst. Korros.* **27**, 506 (1976).
114. A. JOUANNEAU and M. C. PETIT, *J. Chim. Phys.* **73**, 878 (1976).

115. J. R. VILCHE and A. J. ARVÍA, *J. electrochem. Soc.* **123**, 1061 (1976).
116. B. MACDOUGALL and M. COHEN, *J. electrochem. Soc.* **123**, 1783 (1976).
117. M. COHEN and B. MACDOUGALL, *25th Int. Soc. Electrochem.* Meeting, Zürich paper Nr. 91 (1976).
118. T. DICKINSON, A. F. POVEY and P. M. A. SHERWOOD, *J. chem. Soc. Faraday Trans.* I, **73**, 327 (1977).
119. B. MACDOUGALL and M. COHEN, *J. electrochem. Soc.* **124**, 1185 (1977).
120. J. R. VILCHE and A. J. ARVÍA, *Proc. IVth Int. Symp. Passivity*, Airlie, VA. (1977).
121. J. R. VILCHE and A. J. ARVÍA, *Corros. Sci.* **18**, 441 (1978).
122. M. CID, A. JOUANNEAU, D. NGANGA and M. C. PETIT, *Electrochim. Acta* **23**, 945 (1978).
123. B. MACDOUGALL, *J. electrochem. Soc.* **125**, 1883 (1978).
124. B. MACDOUGALL and M. COHEN, *Electrochim. Acta* **23**, 145 (1978).
125. T. OHTSUKA, K. SCHONER and K. E. HEUSLER, *J. electroanal. Chem.* **93**, 171 (1978).
126. M. ZAMIN and M. B. IVES, *J. electrochem. Soc.* **126**, 470 (1979).
127. R. SCHREBLER GUZMÁN, J. R. VILCHE and A. J. ARVIA, *J. electrochem. Soc.* **125**, 1578 (1978).
128. J. R. VILCHE and A. J. ARVÍA, *Corros. Sci.* **15**, 419 (1975).
129. A. J. ARVÍA, *Israel J. Chem.* **18**, 89 (1979).
130. S. SRINIVASAN and E. GILEADI, *Electrochim. Acta* **11**, 321 (1966).
131. N. R. DE TACCONI, J. O. ZERBINO, M. E. FOLQUER and A. J. ARVÍA, *J. electroanal. Chem.* **85**, 213 (1977).